Supplementary Information

Plutonium isotopes as time-markers in South American lake sediments: identifying pre- and post-1959 and French test periods

Floriane Guillevic[1*], Renaldo Gastineau[2,3], Olivier Evrard[4], Pierre Sabatier[3], Amaury Bardelle[4], Pierre-Alexis Chaboche[4], Anthony Foucher[4], Romina Achaga[5], Ana Carolina Ruiz-Fernández[6], Joan-Albert Sanchez-Cabeza[6], Marcos Tassano[7], Mirel Cabrera[7], Juan A. Quicke[8], Guillermo Chalar[9], Maarten Van Daele[10], Valentina Moreno-Allende[11], Jasper Moernaut[11], Torsten Haberzettl[12], José A. Corcho Alvarado[13], Stefan Röllin[13], Hans Sahli[13], Judith Kobler[1], Gerald Dicen[1], Christine Alewell[1]

[1]Environmental Geosciences, University of Basel, Basel, CH-4056, Switzerland
[2]International Research Institute of Disaster Science, Tohoku University, 468-1, Aoba, Aramaki, Aoba-ku, Sendai, Miyagi, 980-8572, Japan
[3]EDYTEM, Université Savoie Mont-Blanc, CNRS, 73376, Le Bourget du Lac, France
[4]Laboratoire des Sciences du Climat et de l'Environnement (LSCE), CEA, CNRS, UVSQ, Université Paris-Saclay, Gif-sur-Yvette 91198, France
[5]Centro de Investigaciones en Física e Ingeniería Del Centro de La Provincia de Buenos Aires (CIFICEN), Universidad Nacional Del Centro de La Pcia. de Bs. As. (UNCPBA), Tandil, Argentina
[6]Unidad Académica Mazatlán, Instituto de Ciencias del Mar y Limnología, Universidad Nacional Autónoma de México, 82040, Mazatlán, Sinaloa, México
[7]Laboratorio de Radioquímica, Área de Radiofarmacia, Centro de Investigaciones Nucleares, Facultad de Ciencias, Universidad de la República, Mataojo 2055, Uruguay
[8]Instituto Nacional de Investigación Agropecuaria (INIA), Ruta 50 Km. 11, Colonia, Uruguay
[9]Sección Limnología, Facultad de Ciencias, Instituto de Ecología y Ciencias Ambientales, Facultad de Ciencias, Universidad de la República, Montevideo, Uruguay.
[10]Renard Centre of Marine Geology, Department of Geology, Ghent University, Ghent, Belgium
[11]Institute of Geology, University of Innsbruck, Innsbruck, Austria
[12]Physical Geography, Institute for Geography and Geology, University of Greifswald, Greifswald, Germany
[13]Spiez Laboratory, Federal Office for Civil Protection, Spiez, Switzerland

*Corresponding author: floriane.guillevic@unibas.ch

Table of content

Text S1: Description of the eight lakes setting

Rincon del Bonete reservoir (Uruguay, 32°S, 56°W)

The Rincon del Bonete reservoir **(RDB)** represents Uruguay's largest freshwater body (**Fig. S1**). Constructed in 1945 for hydroelectric power, its surface area fluctuates between 465-1495 km^2 (Bardelle et al., 2025). The reservoir is located within the Pampa biome and is exposed to a humid subtropical climate, with annual precipitation of 1525 mm on average, peaking in April. The large catchment is mainly covered with natural herbaceous vegetation, and is also covered with cropland, forest plantations, and wetlands. The sediment core was collected near the dam at the deepest depth at the reservoir's southwest end (32.81787 °S, 56.40013 °W) and sub-sampled every 1cm.

La Estanzuela pond (Uruguay, 34°S, 57°W)

La Estanzuela pond (**EST**) is located less than 100 km south of the **RDB** in Uruguay (**Fig. S1**). It was constructed by the Instituto Nacional de Investigación Agropecuaria (INIA) between 1956 and 1957. This small pond (~ 1 km^2) is located within the Pampa biome and is exposed to a humid subtropical climate, with annual precipitation of 1100 mm. The sediment core was collected in the center of the pond (34.34512°S, 57.70864°W) and the core was sub-sampled every 2 cm. **EST** is located in an agricultural area under cultivation for 100 years, which transitioned from plow-based cultivation (1960s-1980s) to livestock-crop rotation and since 2010, no-till farming. A soil core was collected at a reference site near the pond and was analyzed for ^{137}Cs (Tassano et al. 2026) and $^{239+240}Pu$ (this study) giving a value of 367.1 ± 15.9 $Bq.m^{-2}$ (decay corrected to 2026) and 22.5 $Bq.m^{-2}$, respectively.

Lake Melincué (Argentina, 33°S, 61°W)

Lake Melincué (**MEL**) is a shallow, endorheic subsaline lake which is located in the Argentinian Humid Pampa (**Fig. S1**). Its surface area fluctuated between 60 and 110 km^2 over the last decade. Its drainage basin represents an area of 700 km^2, but with a water inflow that is primarily driven by precipitation. The surrounding landscape is dominated by agriculture and cattle raising. The annual precipitation is highly variable, ranging from 501 mm in 2013 and 1177 mm in 2017. Lake Melincué's water levels have experienced significant fluctuations over the past century. Dry conditions from 1900 to 1970 kept levels low, but a marked increase in precipitation after 1976 led to notable rise in lake levels in the 1980s (Guerra et al., 2015; Peralta, 2017). The sediment core was collected in 2016 in the center of the lake, at a water depth of approximately 4 meters (33.69203°S, 61.47399°W).

Lake Barrancosa (Argentina, 37°S, 60°W)

Similarly to MEL, Lake Barrancosa (**BAR**) is also located in the Argentinian Humid Pampa (**Fig. S1**). BAR is a shallow, closed-basin lake with a maximum depth of 5 m and a surface area of 1.7 km^2. Historically, Lake Barrancosa was known for therapeutic baths during the first half of the 20th century. However, major floods in the 1980s altered its water quality and reduced salinity. The wetter period, starting around 1976, coincided with the agricultural expansion in the late 1960s and an intensified production in the 1980s (Plastani et al., 2019, 2025; Achaga et al. 2026)

Lake Ne Luan (Argentina, 41°S, 68°W)

Lake Ne Luan (**NLU**) is a wind-formed, shallow lake on the Argentinian Patagonian plateau (**Fig. S1**), with a maximum depth of 15 m (Temporetti et al., 2014). The sparsely vegetated basin is used for livestock, with the absence of nearby urban settlements. The sediment core was collected in 2019, in the center of the lake (41.50550°S, 68.62670°W).

Lake Laja (Chile, 37°S, 71°W)

Lake Laja (**LAJA**), which is located at 1360 m elevation in the Chilean Andes, has a surface area of 87 km^2 and a maximum depth of 135 m. Since 1958, its water level has been artificially managed for irrigation and the production of hydroelectric power. The catchment (892 km^2) receives 2172 mm of annual precipitation, mostly during the austral winter (Quiroz et al 2005, Urrutia et al. 2010, Van Daele et al. 2015).

Lake Natri (Chile, 42°S, 73°W)

Lake Natri (**NAT**), which is located at 36 m elevation on Chiloé Island in Chile, has a maximum depth of 58 m and a surface area of 7.8 km^2. Its 46.5 km^2 catchment is primarily forested, with mixed native vegetation and natural prairies (Villalobos et al. 2003). The annual precipitation exceeds 2000 mm, with 64% of the total rainfall occurring between April and September (Perez et al., 2009).

Lake Roca Santa Cruz (Argentina, 52°S, 73°W)

Lake Roca (**ROCA**) is located in the Argentinian part of Patagonia in the province of Santa Cruz, has a surface area of 6.7 km² (Bunicontro et al., 2026) and a maximum water depth during coring in 2006 of 38.2 m. **ROCA** is influenced by lake level variations of Lake Argentino which is occasionally dammed by the Perito Moreno glacier, causing lake level rises integrating **ROCA** into Lake Argentino. The sediment core was recovered during a lake level low stand.

Figure S1: Lakes locations within the precipitation (A) and ecoregions (B) maps of southern South America (WorldClim 2.1, Fick and Hijmans, 2017, Ecoregions 2017 © Resolve, Dinerstein et al., 2017).

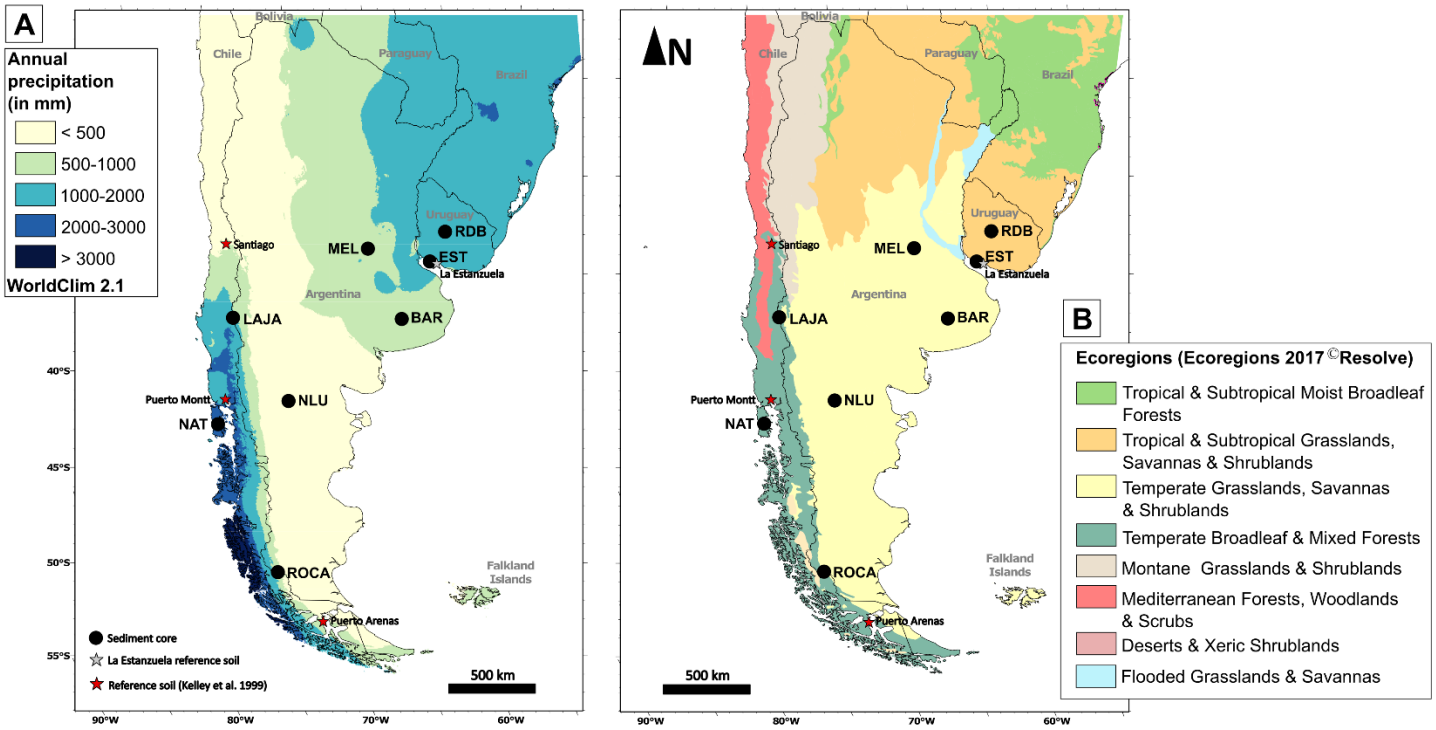

Figure S2: ^{137}Cs deposition ($Bq.m^{-2}$) air filter measurements in Buenos Aires (Tassano et al., 2025)

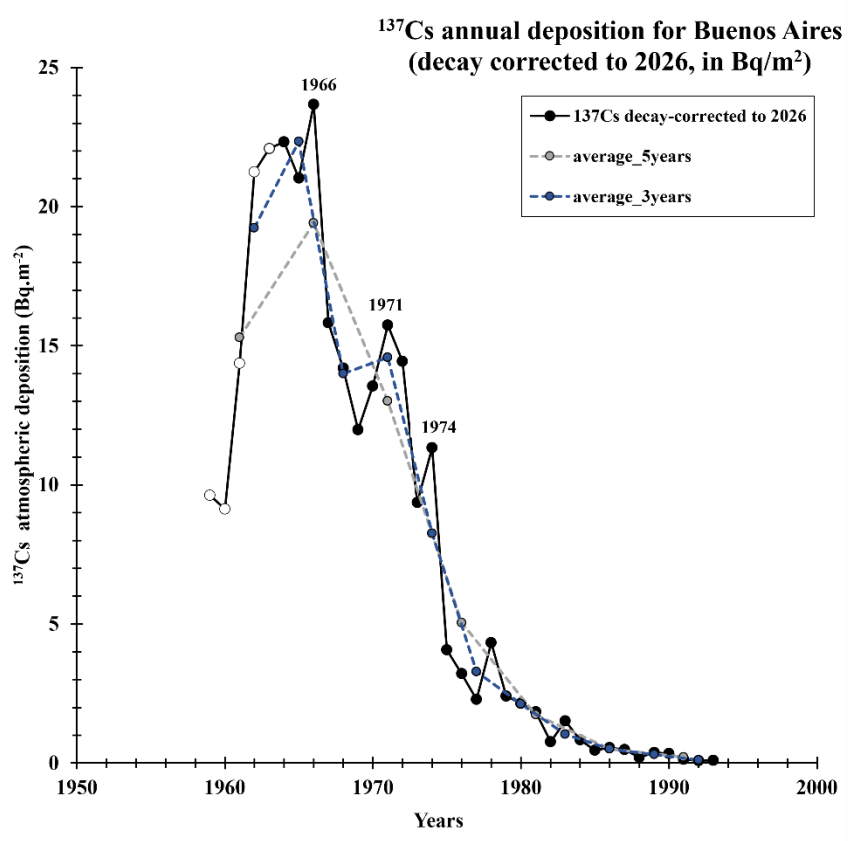

Table S1: Summary of studied lake parameters

	LAT	LONG	Core name	Core length (cm)	Elevation (m)	Ecoregions	Lake area (km^2)	Watershed area (km^2)	Catchment:lake ratio	Maximum depth (m)	Precipitation ($mm.yr^{-1}$)	Coring date	Water salinity	Sub sampling interval (cm)
RDB	32°S	56°W	22BN-01		75	Uruguayan Savanna/ Pampa	465-1485		25-33		1525	2022	freshwater	1
EST	34°S	57°W	INIA02		66	Uruguayan Savanna/ Pampa	0.06	1	17		1100	2022	freshwater	2
MEL	33°S	61°W	Lme 16-2-1	51	84	Humid Pampa	110	700	6	4	501-1177	2016	subsaline	1
BAR	37°S	60°W	LB22-1-2	57.5	245	Humid Pampa	1.65			5	550-1600 (865)	2022	subsaline	1
NLU	41°S	68°W	NLu24-3	151	935	Patagonian Steppe	0.55			10.5	-	2024	saline	1
LAJA	37°S	71°W	LAJ-03	105	1360	Temperate forest Andes Mountains	85	892	10.5	135	2172	2011	freshwater	0.5
NAT	42°S	73°W	1006-11	47.5	36	Valdivian Temperate forest	7.8	46.5	6	58	2000-2500	2023	freshwater	0.5
ROCA	52°S	73°W	RSC06-4	67	179	Subpolar forest	6.7	variable	variable	~40	203	2006	freshwater	1

Figure S3: Comparison of the two methods used for Pu extraction

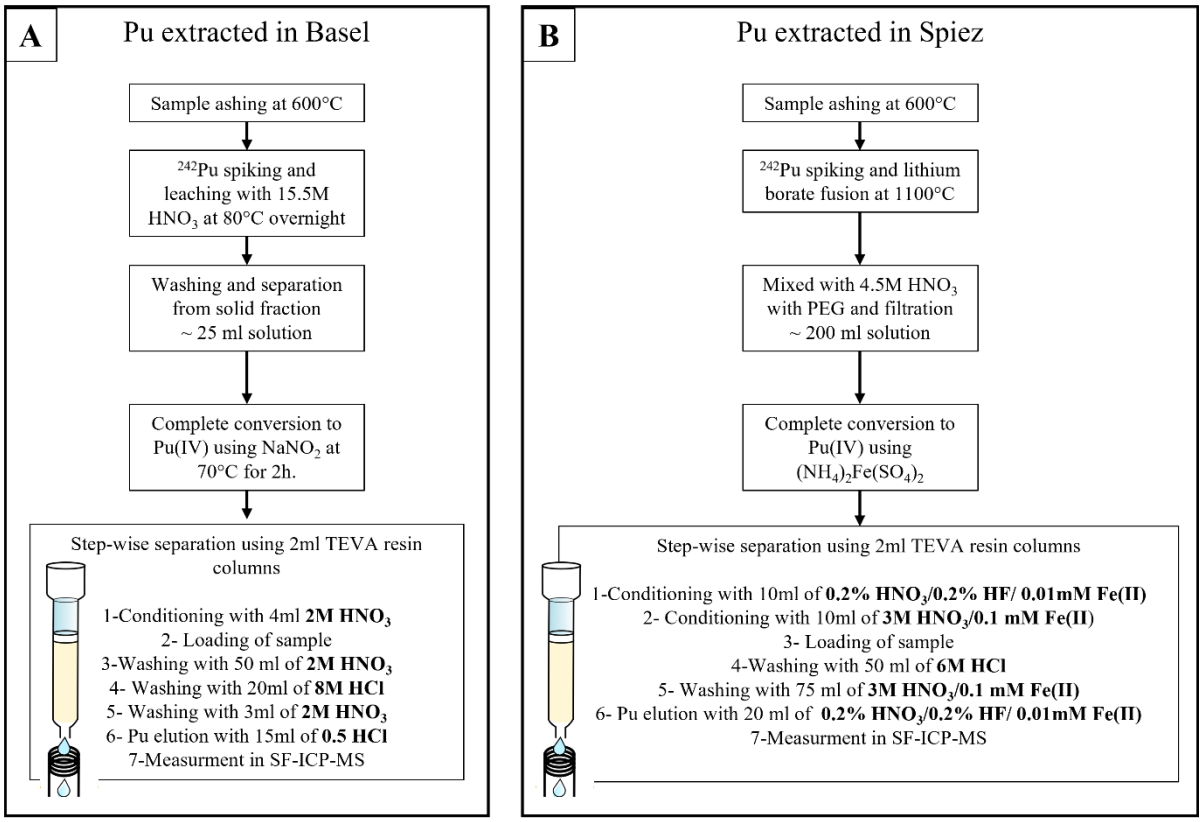

(modified from Ketterer et al. 2004)

(Röllin et al. 2022; Sahli et al. 2017)

Table S2: Measurement parameters to evaluate Pu extraction performance

Lake	Method	Sample weight (g)	Pu recovery (%)	SF Th (min-max)	SF U (min-max)	$^{239+240}$Pu Activity ($Bq \cdot kg^{-1}$)	^{239}Pu ($fg \cdot g^{-1}$)	^{240}Pu ($fg \cdot g^{-1}$)	^{239}Pu/^{240}Pu atom ratio
BAR[1]	A-Basel	2.9-5.0	51- 126	2286- 83998	143- 1100	0.05- 1.54	13.2- 550.9	2.0- 32.6	0.059- 0.188
MEL	A-Basel	4.5-4.9	69-79	15039-129646	374-1462	0.14- 0.76	33.0-266.4	5.3-27.9	0.066-0.236
NAT	A-Basel	0.5-1.2	17- 73	680-21781	480-3073	0.07- 5.04	14.9- 1543.3	3.0- 196.7	0.103-0.253
ROCA	A-Basel	0.7-5.3	65- 86	2885-134541	2257-11148	0.08- 1.25	18.9- 321.6	0.6- 60.4	0.115- 0.277
NLU	B-Spiez	~1	57- 78	10-11035	6436-18875	0.04-0.15	9.8-53.0	1.3-.8	0.053- 0.301
RDB	B-Spiez	~1	87- 114	467-15830	3466-19830	0.14- 1.96	3.6-656.1	0.7- 55.0	0.069- 0.264
EST	B-Spiez	~4	44- 116	542-13822	1405-14890	0.05- 1.12	15.4- 437.0	1.6- 16.0	0.031- 0.194
LAJA	B-Spiez	~1-2	52- 103	684- 28894	761-15612	0.06- 4.15	13.0- 1058.0	1.4- 204.2	0.069- 0.305

[1]The uranium and thorium separation factors were not corrected from gamma measurements; SF: separation factor

Figure S4: ^{137}Cs surface activity and $^{239+240}$Pu surface activity for Lake Barrancosa (BAR), Lake Melincué (MEL) and Lake Natri (NAT). Please note that different half cores were used for ^{137}Cs and $^{239+240}$Pu activity concentration measurement in NAT, and depths were adjusted to align the two half-cores.

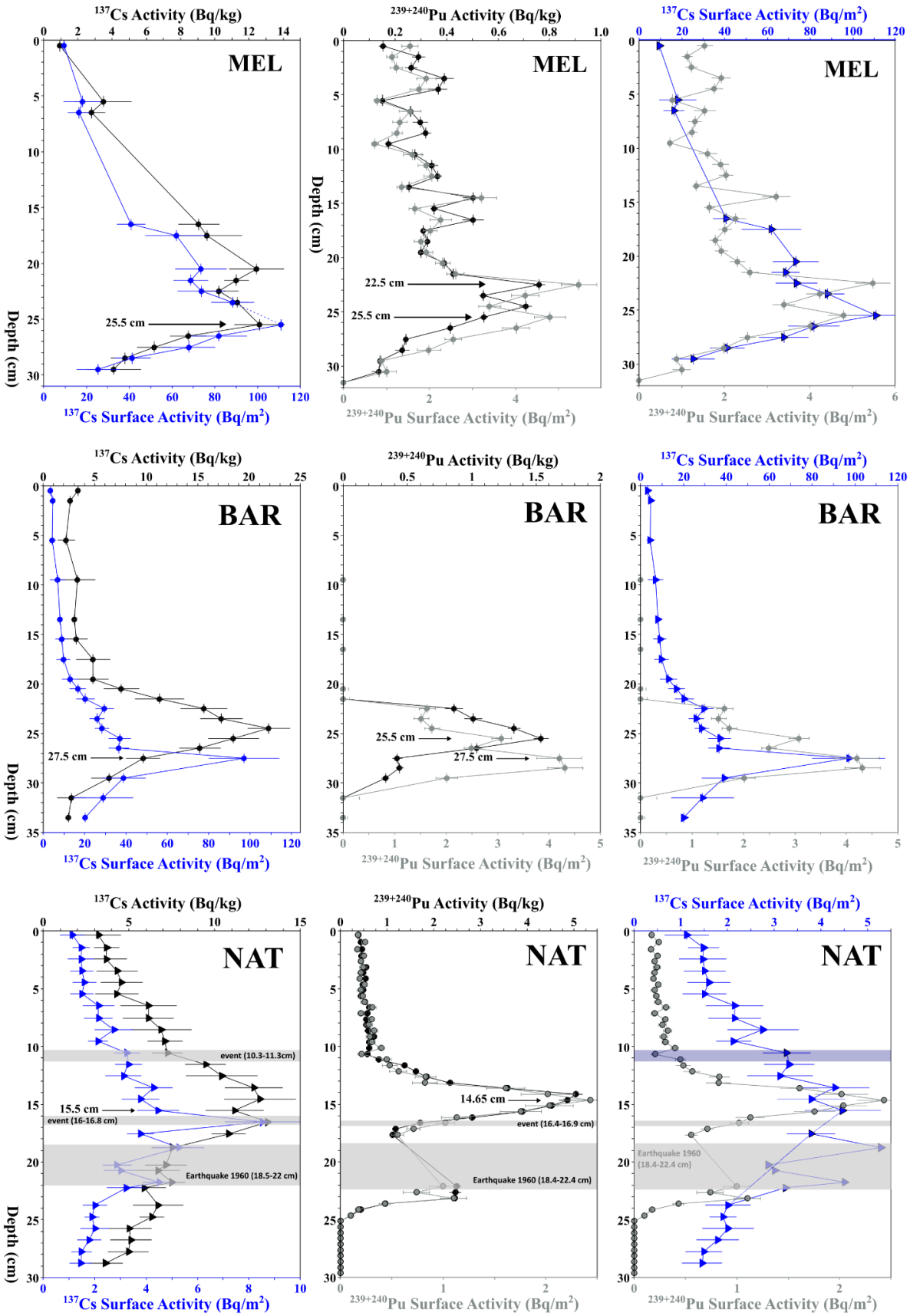

Figure S5: $^{137}Cs/^{239+240}Pu$ activity ratio versus $^{240}Pu/^{239}Pu$ atomic ratio.

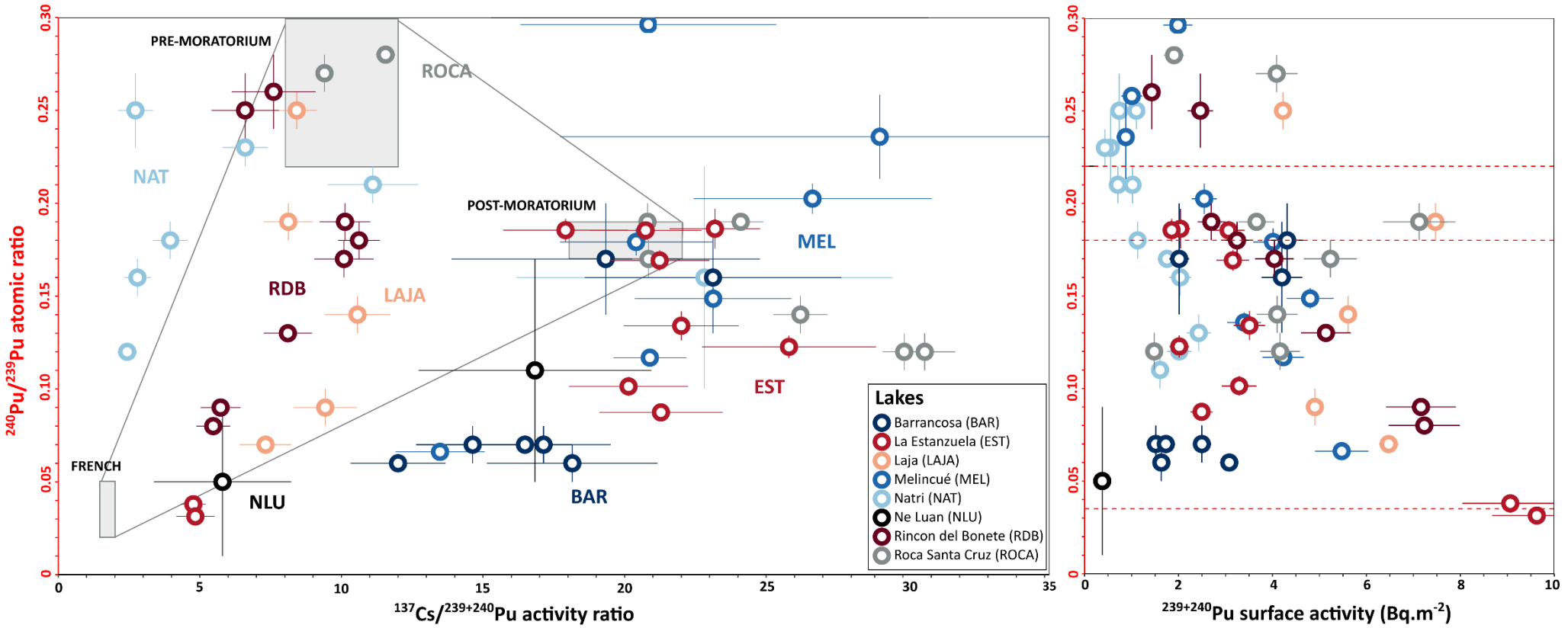

The pre-moratorium end-member ($^{240}Pu/^{239}Pu > 0.22$, $^{137}Cs/^{239+240}Pu = 10 \pm 2$), the post-moratorium end-member ($^{240}Pu/^{239}Pu = 0.18 \pm 0.01$, $^{137}Cs/^{239+240}Pu = 20 \pm 2$) and the French period end-member ($^{240}Pu/^{239}Pu = 0.035 \pm 0.015$, $^{137}Cs/^{239+240}Pu = 1.75 \pm 0.30$)

Figures S6-S13: ^{210}Pb age-depth models for the different lakes.

Figure S6 – Age Depth model for Rincon del Bonete reservoir.

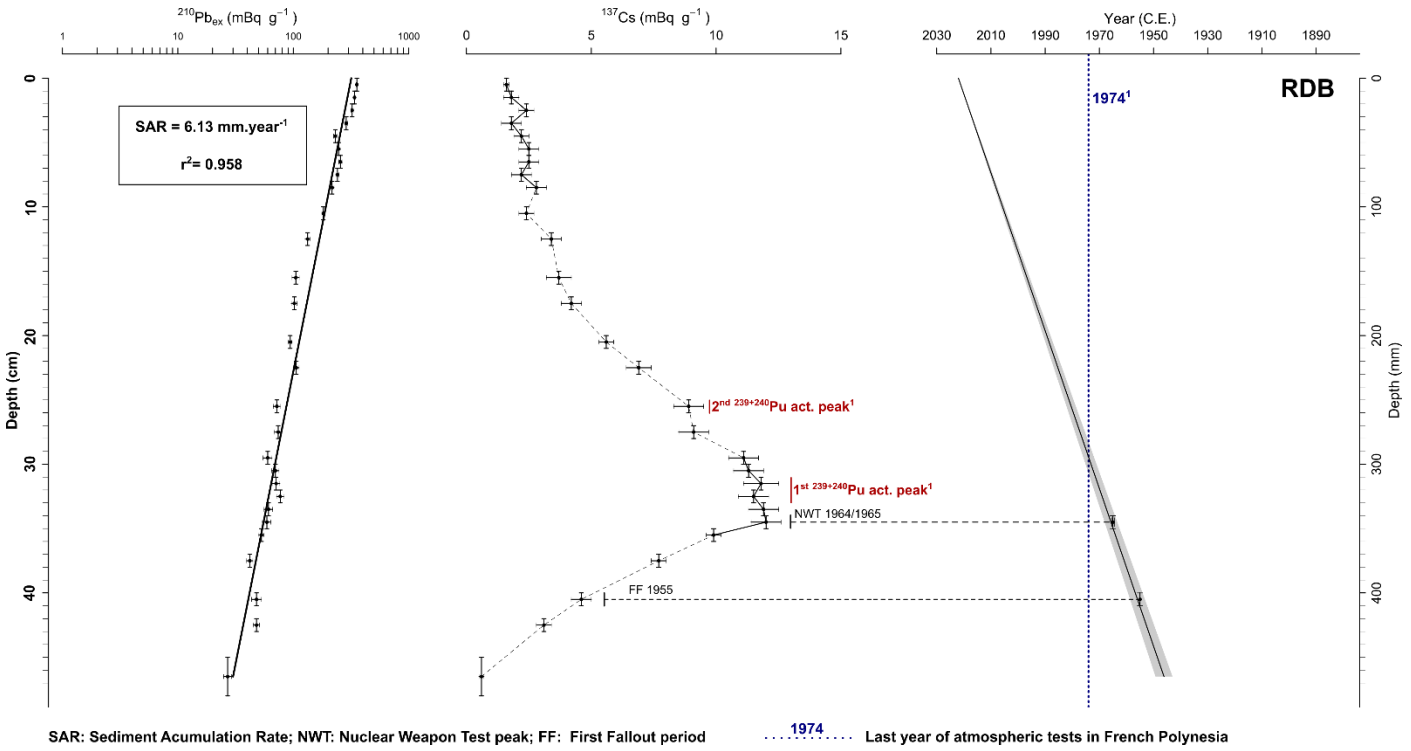

[1]*Colored labels and lines are used for indication purposes only and are not used in the age-depth model.*

The age-depth model for **RDB** was previously published by Bardelle et al. (2025), and the ^{210}Pb$_{ex}$ profile showed a constant exponential decay from the sediment surface down to 45 cm. Since the dam was built around 1945 in good agreement with ^{210}Pb$_{ex}$ chronology, ^{210}Pb$_{ex}$ had not reached equilibrium, making the CRS model inapplicable. The CFCS model was validated by the ^{137}Cs maximum activity of 12 Bq·kg^{-1} at 34 cm. An average sedimentation rate of 0.61±0.02 cm·yr^{-1} was estimated (**Fig. S6**).

Figure S7 – Age-depth model for La Estanzuela pond.

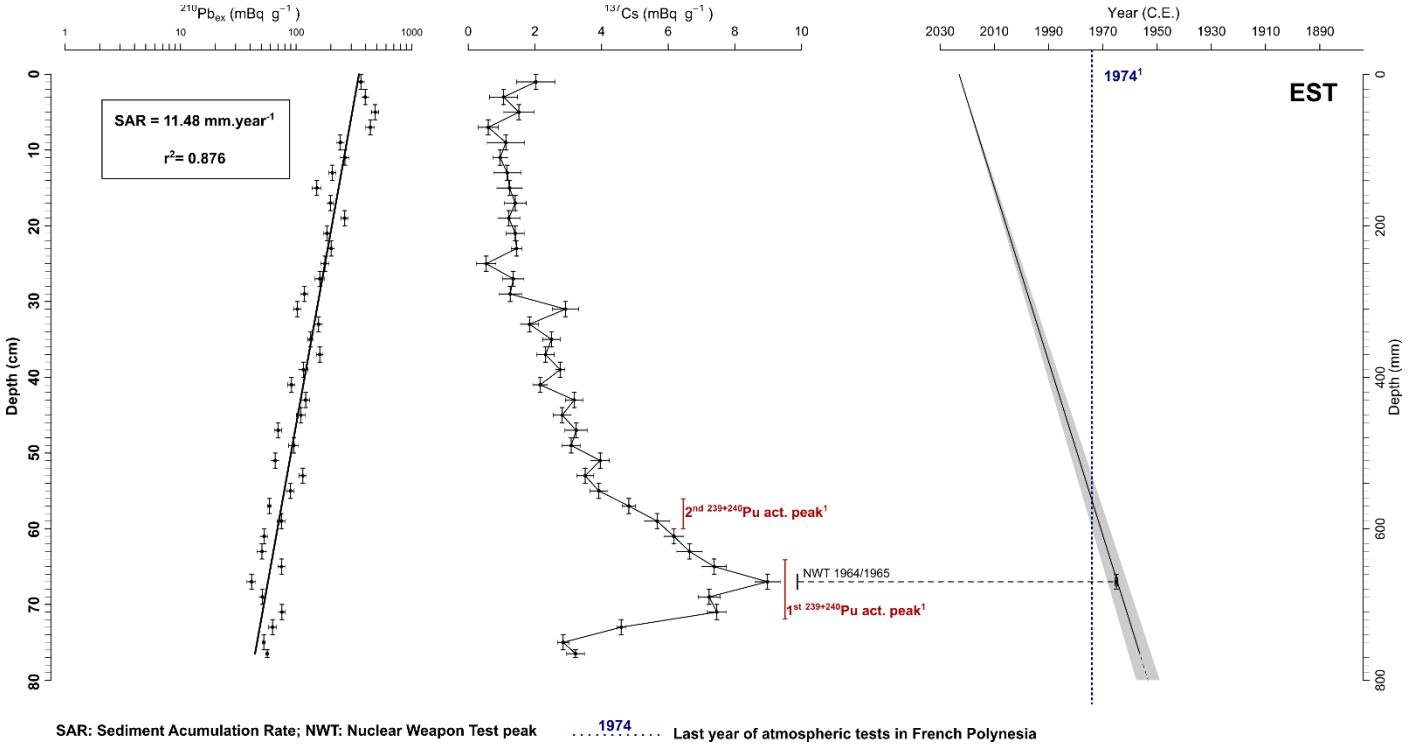

[1]*Colored labels and lines are used for indication purposes only and are not used in the age-depth model.*

For **EST**, the $^{210}Pb_{ex}$ profile showed a constant exponential decay from the surface down to 78 cm, reaching the core bottom. Since the pond was built between 1956 and 1958, in good agreement with the $^{210}Pb_{ex}$ chronology, $^{210}Pb_{ex}$ had not reached equilibrium, making the CRS model inapplicable. The CFCS model was confirmed by the maximum ^{137}Cs activity peak at 69 cm, corresponding to 1964/1965. An average sedimentation rate of 1.15 ± 0.07 cm·yr^{-1} was estimated (**Fig. S7**).

Figure S8 – Age Depth model for Lake Melincué.

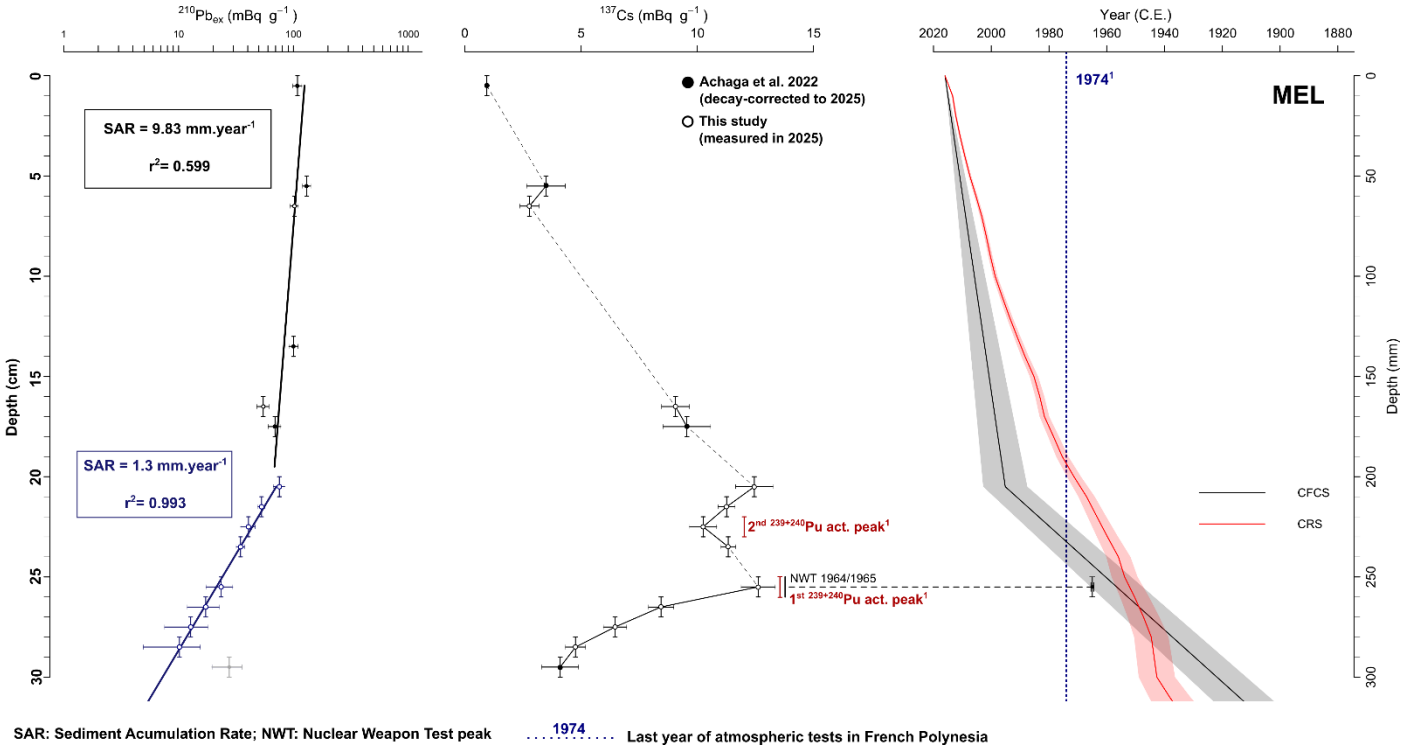

[1]Colored labels and lines are used for indication purposes only and are not used in the age-depth model. Please refer to ***Figure S4*** *for additional information on the depth of the $^{239+240}Pu$ and ^{137}Cs activity peaks, as the activity concentration and surface activity profiles may differ due to density changes.*

For **MEL**, the age-depth model was previously published by Achaga et al. (2022). In this study, additional samples were measured to improve the resolution of the ^{137}Cs peak definition (*white dot*). A drastic change in sedimentation rate was identified at 20.5 cm. The onset of the ^{137}Cs peak at 25.5 cm validates the CFCS model whereas the CRS model estimated ages that were too old.

With the selected CFCS model, a high sedimentation rate of 0.98 ± 0.36 cm·yr^{-1} characterized the upper 20 cm, whereas a 10 times lower rate (0.13 ± 0.01 cm·yr^{-1}) was estimated for the deeper core section using the $^{210}Pb_{ex}$ chronology. This change in the sedimentation rate coincides with a major increase in total organic carbon (TOC) occurring between 22.5 and 20.5 cm, which has been associated with the 1980 flood events and the expansion of the lake area (Achaga et al. 2022). It might also be linked to agricultural expansion that started in the region after the 1970s (Guerra et al., 2015), combined with high-precipitation events that occurred in the late 1970s and beginning to the 1980s (Achaga et al. 2022, Córdoba et al., 2017; Guerra et al., 2015).

In Achaga et al. (2022), this change in sedimentation rate was dated to 1971 ± 3 years using the CRS model, while the updated CFCS model dates the transition at 20.5 cm to 1995 ± 7 years (min-max:1983-2003).

Figure S9 – Age depth model for Lake La Barrancosa.

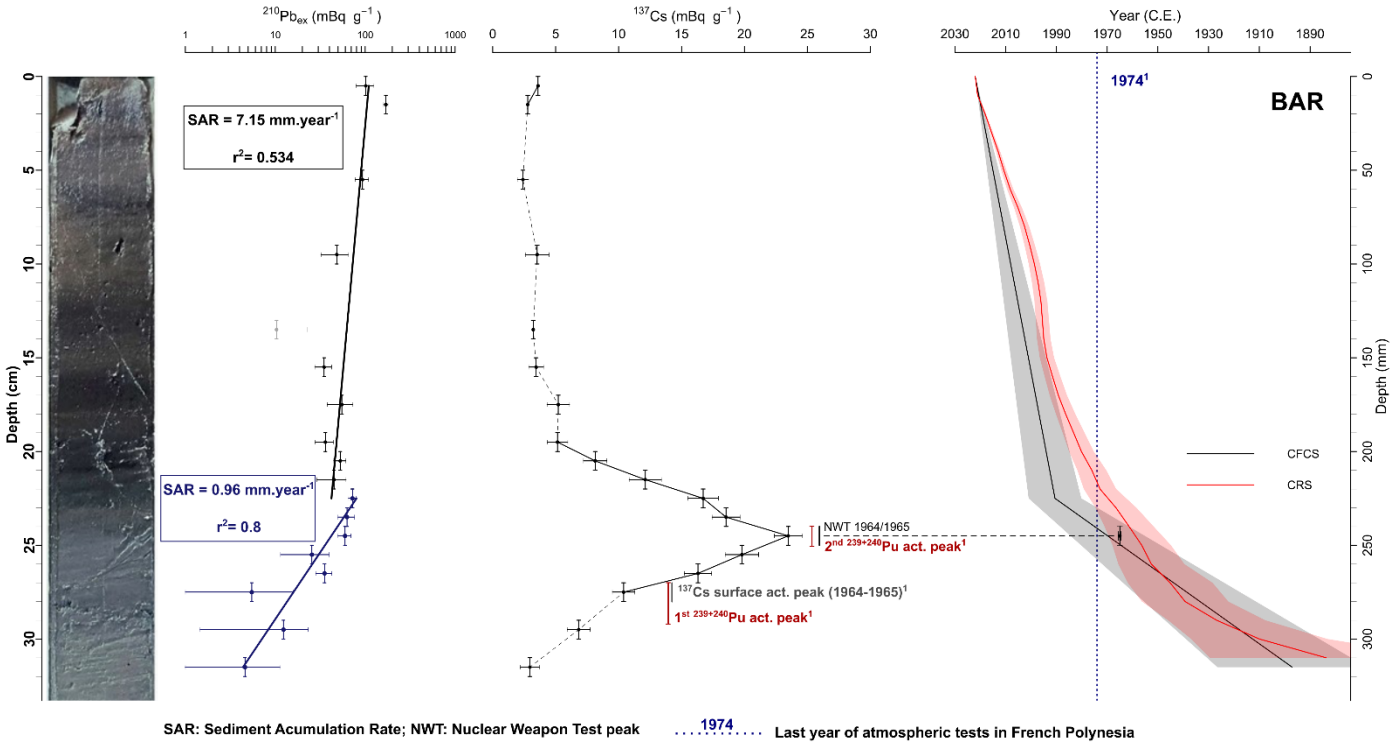

[1]Colored labels and lines are used for indication purposes only and are not used in the age-depth model. Please refer to ***Figure S4*** *for additional information on the depth of the $^{239+240}$Pu and ^{137}Cs activity peaks, as the activity concentration and surface activity profiles may differ due to changes in density.*

The age-depth model for **BAR** was previously published by Achaga et al. (2026, *under review*) using the CRS model. Here, both the CRS and CFCS models are presented here for comparison.

As shown on **Figure S4**, due to significant changes in density around these depths, the ^{137}Cs surface activity peak at 27.5 cm likely corresponds to the maximum 1964 -1965 fallout deposition, rather than the visible ^{137}Cs peak at 24.5 cm. The onset of the ^{137}Cs peak at 27.5 cm validates the CRS model.

Given the strong variability in sedimentation conditions in this shallow lake system (likely driven by changes in water level, precipitation, and land-used in the catchment area), assuming non-constant sedimentation over time is more straightforward. This favors the CRS over the CFCS model.

Figure S10 – Age Depth model for Lake Ne Luan.

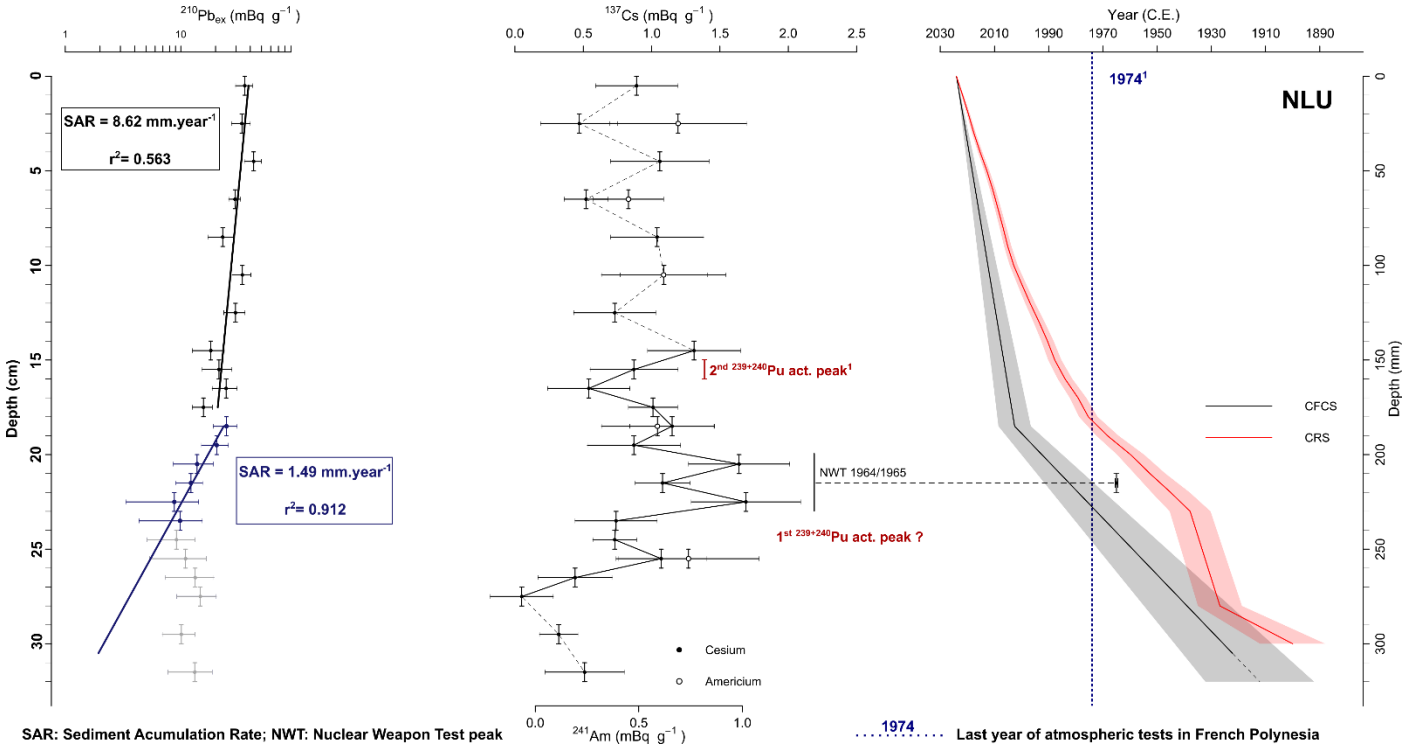

[1]*Colored labels and lines are used for indication purposes only and are not used in the age-depth model.*

For **NLU**, very low $^{210}Pb_{ex}$ activities (< 40 Bq·kg^{-1}) prevent the establishment of a robust chronology. In addition, the very low ^{137}Cs activity concentration (< 1.7 Bq·kg^{-1}), combined with a noisy ^{137}Cs profile, prevents the identification of the ^{137}Cs peak needed to validate the $^{210}Pb_{ex}$ chronology. While a tentative was made to attribute the ^{137}Cs activity peak to the depths 21-23 cm, it did not align with the chronologies provided by either the CFCS or CRS models.

To address these challenges, we considered the $^{239+240}Pu$ data for the NLU age-depth model. The presence of a $^{239+240}Pu$ activity peak at 15.5 cm, characterized by a low $^{240}Pu/^{239}Pu$ atom ratio (**Fig. 2**), aligns with the period of French nuclear testing. Consequently, we opted for the CRS model, which provides an age range at 15.5 cm (Best Age: 1982, Min-Max: 1979-1984) that is closer to the French testing period than the CFCS (Best Age: 2006, Min-Max 2001-2011), without being fully satisfactory.

Figure S11 – Age Depth model for Lake Roca.

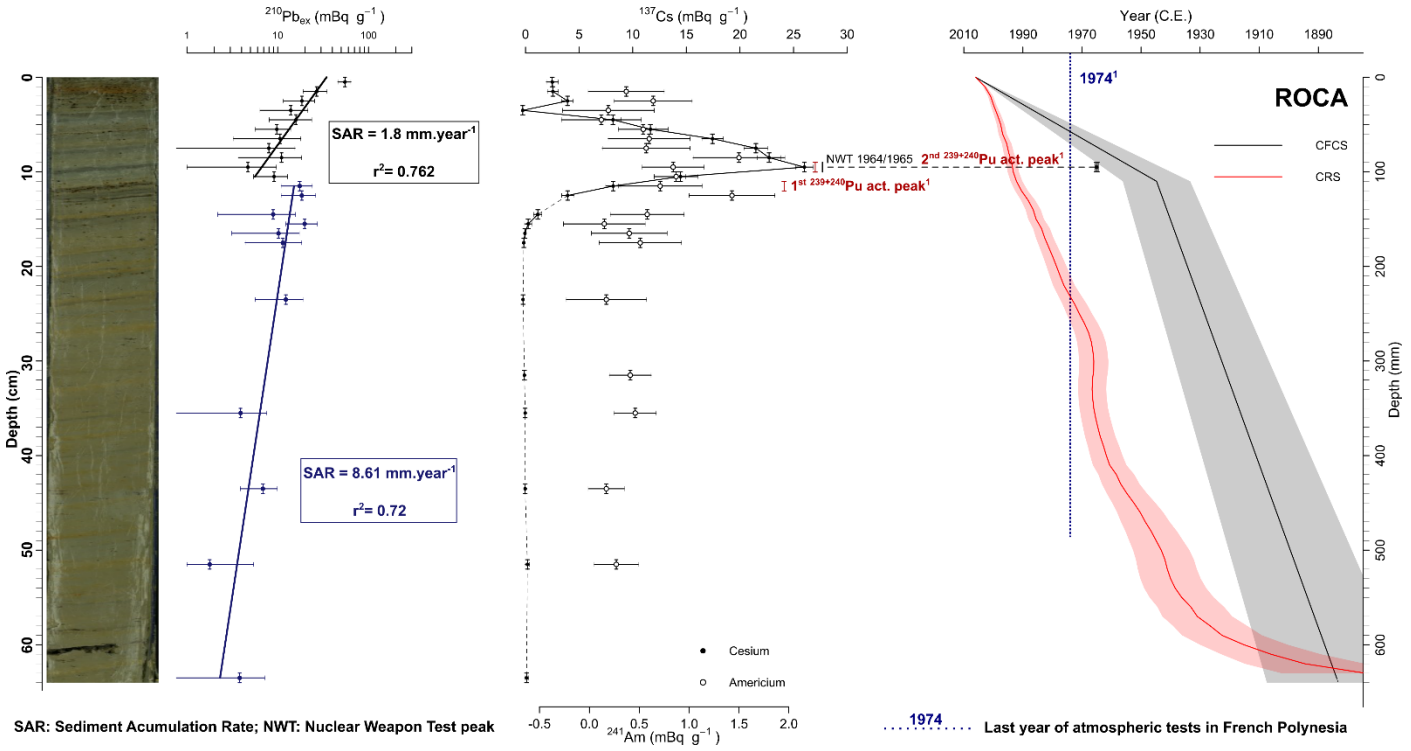

[1]*Colored labels and lines are used for indication purposes only and are not used in the age-depth model.*

For **ROCA**, the $^{210}Pb_{ex}$ profile showed a constant exponential decay from the sediment surface down to 11 cm, marking a transition to a distinct section of the core below 11 cm. This transition indicates a change in the sedimentation rate. The CFCS model was validated by the ^{137}Cs maximum activity of 25 Bq·kg^{-1} observed at 9.5 cm **(Fig. S11)**.

The upper 12 cm of the core shows a sedimentation rate of 0.18 ± 0.03 cm·yr^{-1}, while the deeper section shows a significantly higher rate of 0.86 ± 0.02 cm·yr^{-1}, as estimated from the $^{210}Pb_{ex}$ chronology. This change in sedimentation rate has been set at 11.5 cm, corresponding to an age range of 1932-1956 (BestAge: 1944).

Figure S12 – Age depth model for Lake Laja

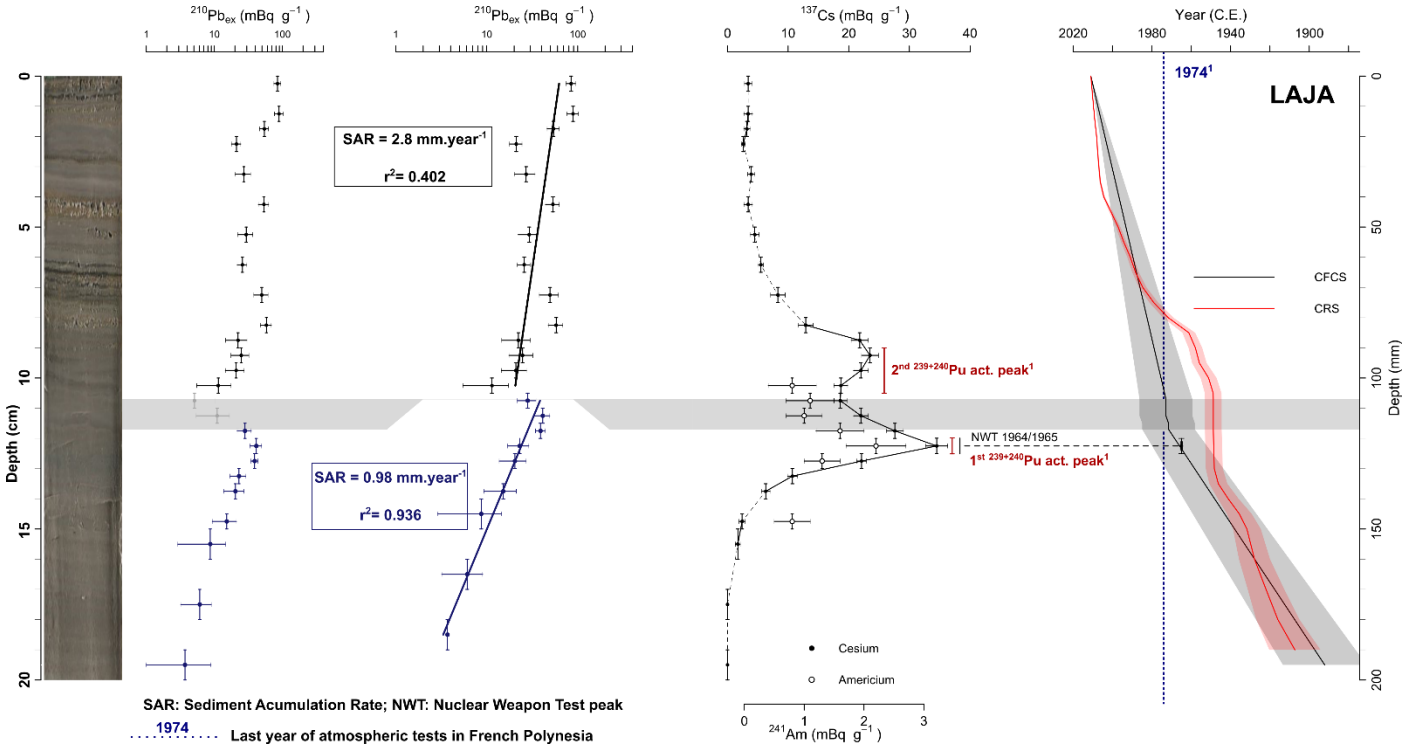

[1]*Colored labels and lines are used for indication purposes only and are not used in the age-depth model.*

For **LAJA**, the upper 10 cm displayed a relatively disturbed $^{210}Pb_{ex}$ profile, likely linked to event deposits visible in the core, yielding to a sedimentation rate of 0.28 ± 0.1 cm·yr^{-1}. Below 12 cm, the $^{210}Pb_{ex}$ profile followed an exponential decay, yielding a sedimentation rate of 0.1 cm.yr^{-1} ± 0.01 (R^2 = 0.94) using the CFCS model. This chronology is validated by a maximum ^{137}Cs activity peak of 35 Bq·kg^{-1} at 12.5 cm.

Figure S13 – Age depth model for Lake Natri

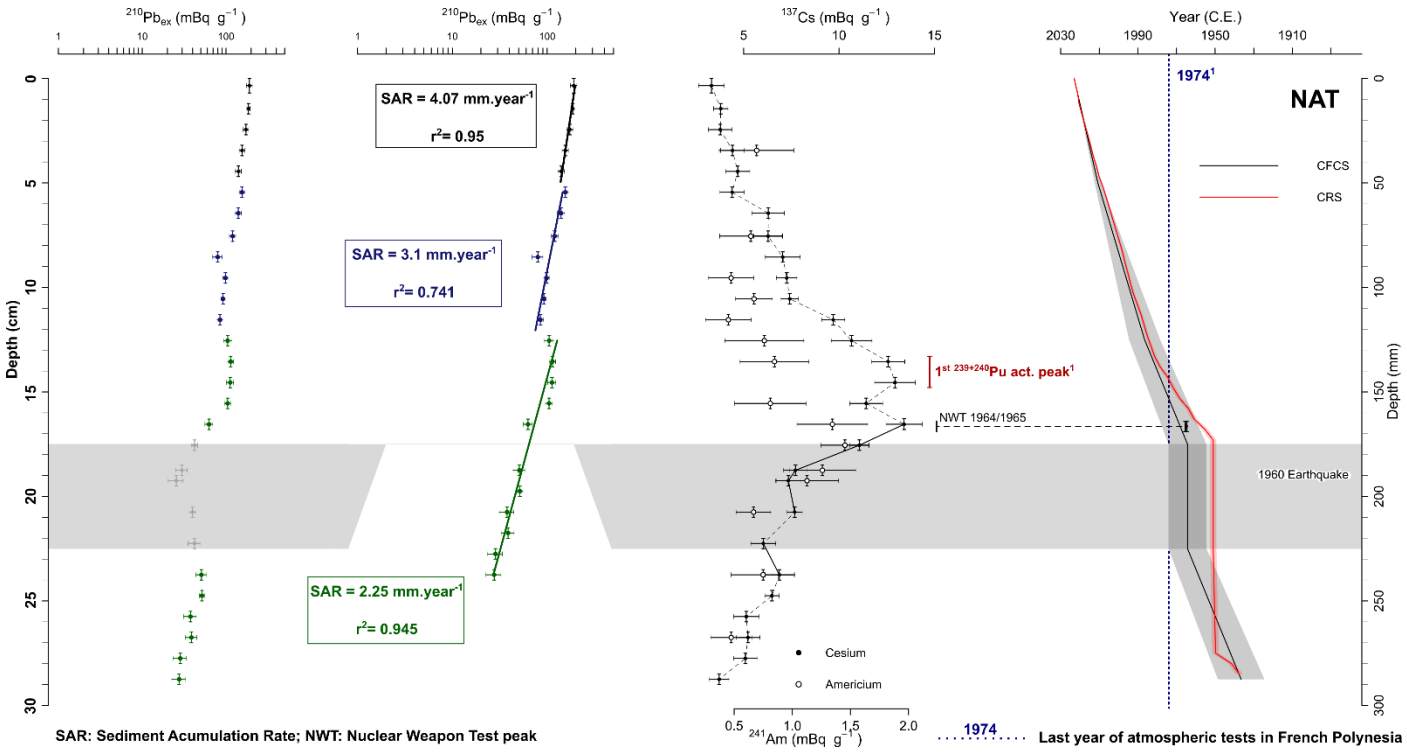

[1]*Colored labels and lines are used for indication purposes only and are not used in the age-depth model.*

For **NAT**, the $^{210}Pb_{ex}$ profile showed an exponential decay with two minor breaks, interpreted as changes in sedimentation rate. From the bottom to the top, sedimentation rates increase from 0.23 cm·yr^{-1} below 12 cm (R^2=0.95) to 0.31 cm·yr^{-1} between 5 and 12 cm (R^2=0.74) and reach 0.41 cm·yr^{-1} in the upper 5 cm (R^2=0.95). The CFCS chronology is well constrained by peaks of ^{137}Cs (13 Bq·kg^{-1}) and ^{241}Am (0.8 Bq·kg^{-1}) detected at 16.7 cm, as well as the historical record of the 1960 (Mw 9.5) earthquake, which corresponds to a major disturbance in the $^{210}Pb_{ex}$ profile between 17 and 22 cm and visually identified as a turbidite.

Table S2: Total and Peak $^{239+240}$Pu inventories with French fallout contribution within the 32-52° latitude band.

	Total Pu inventory I_{total}	**Interval depth**	**Pu Peak inventory** I_{peak}	**Pu peak interval**	**Fraction of FF within** I_{peak}
	(Bq·m^{-2})	**(cm)**	**(Bq·m^{-2})**	**(cm)**	**(%)**
Latitude 30-40[1]	12.6	-	-	-	-
Latitude 40-60[1]	7.2	-	-	-	-
Soil reference **EST** (34°S)	22.3	-	-	-	22.5 ± 0.8
Soil reference Santiago, Chile (33°S)[2]	8.1	-	-	-	44.4 ± 0.7[1]
Soil reference Puerto Montt, Chile (41°S)[2]	7.4	-	-	-	16.3 ± 1.9[1]
Soil reference Punta Arenas, Chile (53°S)[2]	7.0	-	-	-	0 [1]
Rincón del Bonete Reservoir (32°S)	99.8 ± 1.9	0-45	74.0 ± 1.9	24-45	31.1 ± 7.4
La Estanzuela Pond (34°S)	70.2 ± 1.7	0-76	43.9 ± 1.6	54-76	43.3 ± 11.8
Lake Melincué (33°S)	66.2 ± 1.2	0-30	28.3 ± 0.9	22-30	29.9 ± 13.3
Lake Laja (37°S)	39.3 ± 0.5	0-15	30.7 ± 0.5	8.5-13	40.2 ± 13.3
Lake La Barrancosa (37°S)	21.0 ± 0.4	0-30	21.0 ± 0.4	22-30	51.7 ± 13.4
Lake Ñe Luan (41°S)	1.7 ± 0.2	0-25	1.7 ± 0.2	15-25	**n.a**
Lake Natri (42°S)	24.7 ± 0.6	0-25	17.3 ± 0.5	13-25	12.9 ± 6.3
Lake Roca (52°S)	44.5 ± 1.7	0-13	41.1 ± 1.7	5-13	14.7 ± 6.7

[1]median in South America, Dicen et al. 2025 [2] Krey et al. 1976, Kelley et al. 1999: Punta Arenas ^{240}Pu/^{239}Pu = 0.2045 ± 0.005 Puerto Montt ^{240}Pu/^{239}Pu = 0.153 ± 0.001 Santiago ^{240}Pu/^{239}Pu = 0.116 ± 0.002.

References

Achaga, R.V., Irurzun, M.A., Goguitchaichvili, A., Plastani, M.S., Tripaldi, A., Laprida, C., Orgeira, M.J., Mestelán, S., Ruiz Fernández, A.C., Sanchez-Cabeza, J.A., Guyodo, Y., Lagroix, F., Gogorza, C.S.G. Using paleomagnetism to validate the age-depth model of sediment cores from La Barrancosa Lake (Argentina). Quaternary geochronology (under review)

Achaga, R.V., Gogorza, C.S.G., Irurzun, M.A., Gogichaishvili, A., Tripaldi, A., Plastani, M., Laprida, C., Orgeira, M.J., Mestelán, S., Ruiz Fernández, A.C., Sanchez-Cabeza, J.A., Lagroix, F., 2024. Rock magnetic studies on two sediment cores from La Barrancosa lake, Argentina. Latinmag Lett. 143.

Bardelle, A., Gastineau, R., Guillevic, F., Foucher, A., Chaboche, P.-A., Corcho-Alvarado, J.A., Röllin, S., Chalar, G., Sabatier, P., Tassano, M., Cottin, N., Vandromme, R., Cerdan, O., Alewell, C., Evrard, O., 2025. The hidden consequences of agricultural development: Soil degradation and pesticide contamination in the South American Pampa. Sci. Total Environ. 1002, 180584. https://doi.org/10.1016/j.scitotenv.2025.180584

Bunicontro, S.D., Restelli, F.B., Winocur, D.A., Bran, D.M., Lozano, J.G., Menichetti, M., Gutierrez, Y.S., Baradello, L., Lodolo, E., Tassone, A.A., 2026. Neotectonics in Lago Roca, Santa Cruz province, Argentina. J. South Am. Earth Sci. 105992. https://doi.org/10.1016/j.jsames.2026.105992

Córdoba, F.E., Piovano, E.L., Guerra, L., Mulsow, S., Sylvestre, F., Zárate, M., 2017. Independent time markers validate 210Pb chronologies for two shallow Argentine lakes in Southern Pampas. Quat. Int., Analysis of the Quaternary climatic and tectonic forcing along some different tectonic settings of South America 438, 175–186. https://doi.org/10.1016/j.quaint.2016.07.003

Dinerstein, E., Olson, D., Joshi, A., Vynne, C., Burgess, N.D., Wikramanayake, E., Hahn, N., Palminteri, S., Hedao, P., Noss, R., Hansen, M., Locke, H., Ellis, E.C., Jones, B., Barber, C.V., Hayes, R., Kormos, C., Martin, V., Crist, E., Sechrest, W., Price, L., Baillie, J.E.M., Weeden, D., Suckling, K., Davis, C., Sizer, N., Moore, R., Thau, D., Birch, T., Potapov, P., Turubanova, S., Tyukavina, A., de Souza, N., Pintea, L., Brito, J.C., Llewellyn, O.A., Miller, A.G., Patzelt, A., Ghazanfar, S.A., Timberlake, J., Klöser, H., Shennan-Farpón, Y., Kindt, R., Lillesø, J.-P.B., van Breugel, P., Graudal, L., Voge, M., Al-Shammari, K.F., Saleem, M., 2017. An Ecoregion-Based Approach to Protecting Half the Terrestrial Realm. BioScience 67, 534–545. https://doi.org/10.1093/biosci/bix014

Fick, S.E., Hijmans, R.J., 2017. WorldClim 2: new 1-km spatial resolution climate surfaces for global land areas. Int. J. Climatol. 37, 4302–4315. https://doi.org/10.1002/joc.5086

Guerra, L., Piovano, E.L., Cordoba, F.E., Sylvestre, F., Damatto, S., 2015. The hydrological and environmental evolution of shallow Lake Melincue, central Argentinean Pampas, during the last millennium. J. Hydrol. 529, 570–583. https://doi.org/10.1016/j.jhydrol.2015.01.002

Lucía Guerra, Piovano, E.L., Córdoba, F.E., Sylvestre, F., Damatto, S., 2015. The hydrological and environmental evolution of shallow Lake Melincué, central Argentinean Pampas, during the last millennium. J. Hydrol., Advances in Paleohydrology Research and Applications 529, 570–583. https://doi.org/10.1016/j.jhydrol.2015.01.002

Peralta, E.P., 2017. ORDENAMIENTO TERRITORIAL AMBIENTAL DE LA CUENCA HIDROGRÁFICA Y DE APORTE DIRECTO A LA LAGUNA MELINCUÉ.

Plastani, M., Laprida, C., de Oca, F., Massaferro, J., Panarello, H., Mercau, J., Lami, A., 2019. Recent environmental changes inferred from sediments in a shallow lake of the Argentinian pampas. J. Paleolimnol. 61, 37–52. https://doi.org/10.1007/s10933-018-0043-y

Plastani, M.S., Sánchez Vuichard, G., Pisani, N., Berman, A.L., Laprida, C., 2025. Paleolimnological Records in the Central Southern Pampa Plain, in: Piovano, E.L., Stutz, S., Morales, J.A., Ariztegui, D. (Eds.), Pampean Lakes. Springer Nature Switzerland, Cham, pp. 435–464. https://doi.org/10.1007/978-3-031-86028-7_16

Temporetti, P., Beamud, G., Pedrozo, F., 2014. The Trophic State of Patagonian Argentinean Lakes and its Relationship with Depth Distribution in Sediment Phosphorus. Int. J. Environ. Res. 8, 671–686.